Elastic and elasto-optic constants of rutile from a Brillouin scattering study*

M. H. Grimsditch and A. K. Ramdas
Department of Physics, Purdue University, West Lafayette, Indiana 47907
(Received 21 April 1976)

Brillouin scattering in rutile is studied with a triple passed scanning Fabry-Perot interferometer. By observing the spectra with large-order differences between a Brillouin component and its parent laser line, all the elastic moduli c_{ij} were determined with high accuracy; we obtain $c_{11} = 2.674 \pm 0.002$, $c_{33} = 4.790 \pm 0.002$, $c_{44} = 1.233 \pm 0.008$, $c_{66} = 1.894 \pm 0.015$, $c_{12} = 1.808 \pm 0.037$, and $c_{13} = 1.466 \pm 0.029$ in units of 10^{12} dyn/cm^2. Elasto-optic constants p_{ijkl} of rutile are deduced from an intercomparison of its Brillouin components with those of fused quartz as well as from the intensity ratios of the Brillouin components observed with a variety of scattering geometries. These constants are determined as a function of wavelength and show interesting dispersion effects. We have verified for the first time the recent prediction of Anastassakis and Burstein that $p_{ijkl} \neq p_{jikl}$ by obtaining $p_{zyzy}/p_{yzzy} = 1.16 \pm 0.06$. We have also confirmed the prediction by Nelson and Lax and the observations of Nelson and Lazay regarding the inequality $p_{ijkl} \neq p_{ijlk}$. By measuring the Brillouin spectra and the 447-cm^{-1} E_g Raman line under identical experimental conditions with a double monochromator, we have determined the absolute value of the single independent component characterizing the Raman tensor per unit cell, viz., $|d| = 22 \pm 2$ Å^2.

I. INTRODUCTION

It is now well established that Brillouin scattering is an effective experimental technique for determining elastic and elasto-optic constants of crystals.[1,2] Using this technique we recently determined[3] the elastic constants of diamond with very high precision and also deduced all the elasto-optic constants including their wavelength dependence. In this paper we present our results on the Brillouin scattering in rutile. We have investigated this crystal in view of a number of interesting aspects of the phenomenon resulting from (a) large birefringence,[4-6] (b) dispersion of optical properties in the visible spectrum,[4] (c) the symmetry of the elasto-optic tensor as reformulated by Nelson and Lax[7] and Anastassakis and Burstein,[8] and (d) large elastic moduli which permit high precision in their determination.

II. EXPERIMENTAL

The rutile samples were cut from a boule free from Al_2O_3 obtained from the National Lead Co.[9] Samples of various geometries were oriented with x rays, cut and polished to within ~ 2° from the specified orientations. The sample of fused quartz used as a scattering intensity standard was of Suprasil grade obtained from Amersil, Inc.[10] The equipment and the experimental procedures used have been described elsewhere[3,11]; besides the two sets of matched etalon plates described in Ref. 3, a third pair with (98 ± 0.5)% reflectivity in the range 4500–5500 Å was used in some of the experiments. All the experiments in this investigation were performed at ~ 23 °C.

III. THEORY

The theory of Brillouin scattering requires a complete specification of the tensors characterizing the elasto-optic constants (p_{ijkl}) and the elastic moduli (c_{ijkl}). Traditionally, the symmetry of these tensors is derived assuming that the stress and strain tensors are symmetric.[12] These assumptions were questioned by Laval,[13] Viswanathan,[14] and Raman and Viswanathan,[15] and, more recently, by Nelson and Lax[7] and Anastassakis and Burstein.[8] More specifically, Nelson and Lax[7] predicted that "rotations of volume elements within an acoustic wave can make a large contribution to the scattering of light from an acoustic shear wave in optically anisotropic media, thus removing the traditionally assumed symmetry between the last two (acoustic) indices of the usual photoelastic tensor p_{ijkl}." Nelson and Lazay[16,17] and Nelson, Lazay, and Lax[6] verified this prediction in a spectacular fashion in rutile and calcite, respectively. It is useful to comment here on the implications of the nonsymmetric strain for the symmetry of the elastic moduli. Lax[18] has recently discussed this problem and has concluded that the usual 21-constant theory of elastic moduli is adequate, "rotational" effects playing no significant role. The following simple argument may be advanced to clarify this point. It is easy to show that for long-wavelength transverse phonons the components of stress satisfy $(\sigma_{ij} - \sigma_{ji})/\sigma_{ij} \sim l^2/\lambda^2$, where l is on the order of the unit-cell dimensions and λ is the wavelength of the phonon; thus $\sigma_{ij} = \sigma_{ji}$ is an excellent approximation when $\lambda \gg l$. Energy considerations taken together with this equality lead to the traditional symmetry of c_{ijkl}. It should be re-

TABLE I. Elastic moduli for crystals of $D_{4h}(\frac{4}{m}\frac{2}{m}\frac{2}{m})$ point group.

$$\begin{bmatrix} c_{11} & c_{12} & c_{13} & 0 & 0 & 0 \\ c_{12} & c_{11} & c_{13} & 0 & 0 & 0 \\ c_{13} & c_{13} & c_{33} & 0 & 0 & 0 \\ 0 & 0 & 0 & c_{44} & 0 & 0 \\ 0 & 0 & 0 & 0 & c_{44} & 0 \\ 0 & 0 & 0 & 0 & 0 & c_{66} \end{bmatrix}$$

marked here that the above discussion on the elasto-optic tensor p_{ijkl} assumes the symmetry arising from the interchange of i and j, the indices characterizing the dielectric tensor. Anastassakis and Burstein[8] have recently proposed that in Brillouin scattering where frequency shifts are involved, this assumption need not hold.

In Tables I and II the elastic and elasto-optic constants for rutile (D_{4h} symmetry) derived on the basis of the above discussion are given. The contracted two index notation of Ref. 7 ($xx \to 1$, $yy \to 2$, $zz \to 3$, $yz \to 4$, $zy \to \bar{4}$, $zx \to 5$, $xz \to \bar{5}$, $xy \to 6$, and $yx \to \bar{6}$) is used for the elasto-optic constants.

As is well known, Brillouin scattering can be viewed as a Bragg reflection from the optical stratifications produced by the long-wavelength acoustic waves, the frequency shifts being due to the Doppler affect associated with the "moving mirrors." In Fig. 1, we present a schematic view of Brillouin scattering in a birefringent medium, following the treatment given by Chandrasekharan.[5] It can be seen that the ordinary law of "reflection" has to be modified according to

$$n_i \cos\theta_i = n_s \cos\theta_s , \tag{1}$$

where i,s refer to the incident and scattered directions, θ_i and θ_s are the glancing angles with respect to the stratifications, and n_i and n_s are the corresponding refractive indices. Thus, in general, the phonon propagation direction will not be along the bisector of the incident and scattered directions. The frequency shifts of the Brillouin components are given by

$$\Delta\omega = \pm \omega_L (v_s/c)(n_i^2 + n_s^2 - 2n_i n_s \cos\theta)^{1/2}, \tag{2}$$

where ω_L is the frequency of the exciting laser, v_s is the velocity of propagation of the sound wave producing the scattering, c is the velocity of light in vacuum, and θ is the scattering angle; v_s can be written $(X/\rho)^{1/2}$, where X is an appropriate combination of the elastic moduli and ρ is the density. Table III gives the values of X for different propagation directions of the sound waves.

TABLE II. Elasto-optic constants for crystals of $D_{4h}(\frac{4}{m}\frac{2}{m}\frac{2}{m})$ point group.

$$\begin{bmatrix} p_{11} & p_{12} & p_{13} & 0 & 0 & 0 & 0 & 0 & 0 \\ p_{12} & p_{11} & p_{13} & 0 & 0 & 0 & 0 & 0 & 0 \\ p_{31} & p_{31} & p_{33} & 0 & 0 & 0 & 0 & 0 & 0 \\ 0 & 0 & 0 & p_{44} & p_{4\bar{4}} & 0 & 0 & 0 & 0 \\ 0 & 0 & 0 & p_{\bar{4}4} & p_{\bar{4}\bar{4}} & 0 & 0 & 0 & 0 \\ 0 & 0 & 0 & 0 & 0 & p_{4\bar{5}} & p_{\bar{4}4} & 0 & 0 \\ 0 & 0 & 0 & 0 & 0 & p_{4\bar{4}} & p_{44} & 0 & 0 \\ 0 & 0 & 0 & 0 & 0 & 0 & 0 & p_{66} & p_{6\bar{6}} \\ 0 & 0 & 0 & 0 & 0 & 0 & 0 & p_{6\bar{6}} & p_{66} \end{bmatrix}$$

The intensity of light scattered by a sound wave is given by

$$I = \text{const}\ \frac{(\hat{e}_s \cdot \underline{T} \cdot \hat{e}_i)^2}{X} , \tag{3}$$

where $\hat{e}_s$ and $\hat{e}_i$ are unit vectors along the polarization direction of the scattered and incident light, respectively, and $\underline{T}$ is the scattering tensor characterizing the sound wave under consideration. The components of the scattering tensor, referred to the axes in which the dielectric tensor is diagonal, are given by

$$T_{ij} = \sum_{k,l} \epsilon_{ii}\epsilon_{jj} p_{ijkl} \beta_k \alpha_l , \quad i,j,k,l = x,\ y,\ \text{or}\ z. \tag{4}$$

Here ϵ_{ii} and ϵ_{jj} are the principal dielectric con-

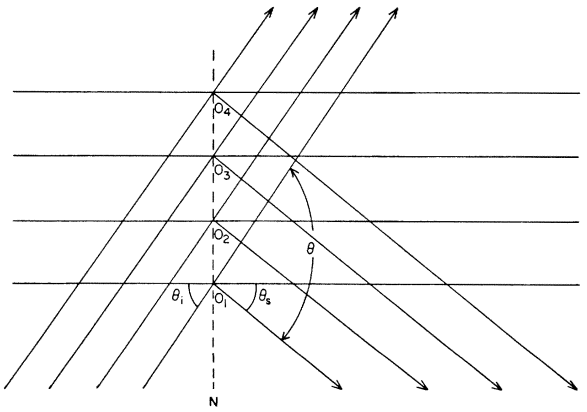

FIG. 1. Brillouin scattering in a birefringent medium. The incident and scattered radiations make glancing angles θ_i and θ_s, respectively, with the stratifications produced by the sound wave, and $\theta = \theta_i + \theta_s$ is the angle through which the radiation is scattered; ON, the normal to the stratifications, is the direction of propagation of the sound wave.

TABLE III. Scattering tensor ($\underline{T}$), $X=v_s^2\rho$, and the polarization vector ($\vec{u}$) of phonons traveling along $\vec{q}$; the entries in the columns for $\vec{q}$ and $\vec{u}$ are their direction cosines. L, T, QL, and QT denote longitudinal, transverse, quasilongitudinal, and quasitransverse, respectively. The two index notation for the p_{ij}'s is explained in the text.

$\vec{q}$	X	$\underline{T}$	$\vec{u}$
$(1,0,0)$	c_{11}	$2\begin{bmatrix} n_o^4 p_{11} & 0 & 0 \\ 0 & n_o^4 p_{12} & 0 \\ 0 & 0 & n_e^4 p_{31} \end{bmatrix}$	$(1,0,0)$: L
	c_{66}	$2\begin{bmatrix} 0 & n_o^4 p_{6\bar{6}} & 0 \\ n_o^4 p_{66} & 0 & 0 \\ 0 & 0 & 0 \end{bmatrix}$	$(0,1,0)$: T
	c_{44}	$2\begin{bmatrix} 0 & 0 & n_o^2 n_e^2 p_{4\bar{4}} \\ 0 & 0 & 0 \\ n_o^2 n_e^2 p_{\bar{4}4} & 0 & 0 \end{bmatrix}$	$(0,0,1)$: T
$(0,0,1)$	c_{33}	$2\begin{bmatrix} n_o^4 p_{13} & 0 & 0 \\ 0 & n_o^4 p_{13} & 0 \\ 0 & 0 & n_e^4 p_{33} \end{bmatrix}$	$(0,0,1)$: L
	c_{44}	$2\begin{bmatrix} 0 & 0 & 0 \\ 0 & 0 & n_o^2 n_e^2 p_{44} \\ 0 & n_o^2 n_e^2 p_{\bar{4}4} & 0 \end{bmatrix}$	$(0,1,0)$: T
	c_{44}	$2\begin{bmatrix} 0 & 0 & n_o^2 n_e^2 p_{44} \\ 0 & 0 & 0 \\ n_o^2 n_e^2 p_{\bar{4}4} & 0 & 0 \end{bmatrix}$	$(1,0,0)$: T
$\left(\frac{1}{\sqrt{2}},\frac{1}{\sqrt{2}},0\right)$	$\frac{1}{2}(c_{11}+c_{12}+2c_{66})$	$\begin{bmatrix} n_o^4(p_{11}+p_{12}) & n_o^4(p_{66}+p_{6\bar{6}}) & 0 \\ n_o^4(p_{66}+p_{6\bar{6}}) & n_o^4(p_{11}+p_{12}) & 0 \\ 0 & 0 & 2n_e^4 p_{31} \end{bmatrix}$	$\left(\frac{1}{\sqrt{2}},\frac{1}{\sqrt{2}},0\right)$: L
	$\frac{1}{2}(c_{11}-c_{12})$	$\begin{bmatrix} n_o^4(p_{11}-p_{12}) & n_o^4(p_{66}-p_{6\bar{6}}) & 0 \\ -n_o^4(p_{66}-p_{6\bar{6}}) & -n_o^4(p_{11}-p_{12}) & 0 \\ 0 & 0 & 0 \end{bmatrix}$	$\left(\frac{1}{\sqrt{2}},-\frac{1}{\sqrt{2}},0\right)$: T
	c_{44}	$\sqrt{2}\begin{bmatrix} 0 & 0 & n_o^2 n_e^2 p_{4\bar{4}} \\ 0 & 0 & n_o^2 n_e^2 p_{4\bar{4}} \\ n_o^2 n_e^2 p_{\bar{4}4} & n_o^2 n_e^2 p_{\bar{4}4} & 0 \end{bmatrix}$	$(0,0,1)$: T
$\left(\frac{1}{\sqrt{2}},0,\frac{1}{\sqrt{2}}\right)$	$\frac{1}{2}(R+\sqrt{L})$ [b,c]	a	a: QL
	$\frac{1}{2}(R-\sqrt{L})$	a	a: QT
	$\frac{1}{2}(c_{66}+c_{44})$	$\sqrt{2}\begin{bmatrix} 0 & n_o^4 p_{6\bar{6}} & 0 \\ n_o^4 p_{66} & 0 & n_o^2 n_e^2 p_{44} \\ 0 & n_o^2 n_e^2 p_{\bar{4}4} & 0 \end{bmatrix}$	$(0,1,0)$: T

TABLE III. *(Continued)*

$\vec{q}$	X	$\underline{T}$	$\vec{u}$
	$\frac{1}{2}(M+\sqrt{N})$ [d,e]	**a**	**a**: QL
$\left(\frac{1}{2},\frac{1}{2},\frac{1}{\sqrt{2}}\right)$	$\frac{1}{2}(M-\sqrt{N})$	**a**	**a**: QT
	$\frac{1}{4}(c_{11}+2c_{44}-c_{12})$	$\begin{bmatrix} \frac{n_o^4(p_{11}-p_{12})}{\sqrt{2}} & \frac{n_o^4(p_{66}-p_{6\bar{6}})}{\sqrt{2}} & n_o^2 n_e^2 p_{44} \\ \frac{-n_o^4(p_{66}-p_{6\bar{6}})}{\sqrt{2}} & \frac{-n_o^4(p_{11}-p_{12})}{\sqrt{2}} & -n_o^2 n_e^2 p_{44} \\ n_o^2 n_e^2 p_{\bar{4}4} & -n_o^2 n_e^2 p_{\bar{4}4} & 0 \end{bmatrix} \left(\frac{1}{\sqrt{2}},-\frac{1}{\sqrt{2}},0\right)$: T

[a] Indicates that the vector or tensor depends on the c_{ij}'s.
[b] $R=\frac{1}{2}(c_{11}+c_{33})+c_{44}$.
[c] $L=\frac{1}{4}(c_{11}-c_{33})^2+(c_{13}+c_{44})^2$.
[d] $M=\frac{1}{4}(c_{11}+2c_{33}+c_{12}+4c_{44}+2c_{66})$.
[e] $N=\frac{1}{16}(c_{11}-2c_{33}+c_{12}+2c_{66})^2+(c_{13}+c_{44})^2$.

stants, and β_k and α_l are the direction cosines of the polarization and propagation vectors of the phonon, respectively. The scattering tensors for phonons along various crystallographic directions are presented in Table III.

In the application of the above theory to the analyses of experimental data, a number of important points should be borne in mind. (i) As a consequence of the birefringence, the phonon propagation direction may not coincide with the bisector of the incident and the scattered directions. (ii) It should be noted that $\hat{e}_i$ and $\hat{e}_s$ in Eq. (3), the polarization vectors of the incident and scattered light, may not be normal to the wave vector of the light, though they are always so with respect to Poynting's vector. It turns out that effects arising from this are important even for directions of incidence and scattering normal to the crystal surfaces. (iii) In intensity calculations, it is necessary to consider such factors as solid-angle expansion, scattering-

TABLE IV. Intensities (I) of Brillouin components for (a) light incident along $\vec{k}_i \| (1/\sqrt{2})(\bar{1},1,0)$ and scattered along $\vec{k}_s \| (1/\sqrt{2})(1,1,0)$ and (b) $\vec{k}_i \| (1,0,0)$ and $\vec{k}_s \| (0,\bar{1},0)$. H (horizontal) and V (vertical) denote the polarizations relative to the horizontal scattering plane. Superscript and subscript refer to the scattered and incident polarizations, respectively. For case (a) the phonon propagation directions ($\vec{q}$) are (1,0,0) for I_V^V and I_H^H, and (cos3.2°, ±sin3.2°, 0) for I_H^V and I_V^H, respectively. For case (b) $\vec{q} \| (1/\sqrt{2})(1,1,0)$ for I_V^V and I_H^H, (sin41.8°, cos41.8°, 0) for I_H^V, and (cos41.8°, sin41.8°, 0) for I_V^H. The vector $\vec{u}$ denotes the polarization of the phonon when it propagates along the bisector.

	$\vec{u}$	I_V^V	I_V^H	I_H^V	I_H^H
	L(1,0,0)	$\frac{4n_e^8 p_{31}^2}{c_{11}}$	0	0	$\frac{n_o^8(p_{11}-p_{12})^2}{c_{11}}$
(a)	T_1(0,1,0)	0	0	0	$\frac{4n_o^8(p_{66}-p_{6\bar{6}})^2}{c_{66}}$
	T_2(0,0,1)	0	$\frac{2.223 n_e^4 n_o^4 p_{4\bar{4}}^2}{c_{44}}$	$\frac{2.223 n_e^4 n_o^4 p_{\bar{4}4}}{c_{44}}$	0
	$L\frac{1}{\sqrt{2}}(1,1,0)$	$\frac{8n_e^8 p_{31}^2}{c_{11}+c_{12}+2c_{66}}$	0	0	$\frac{2n_o^8(p_{66}+p_{6\bar{6}})^2}{c_{11}+c_{12}+2c_{66}}$
(b)	$T_1\frac{1}{\sqrt{2}}(1,\bar{1},0)$	0	0	0	$\frac{2n_o^8(p_{66}-p_{6\bar{6}})^2}{c_{11}-c_{12}}$
	T_2(0,0,1)	0	$\frac{2.223 n_e^4 n_o^4 p_{4\bar{4}}^2}{c_{44}}$	$\frac{2.223 n_e^4 n_o^4 p_{\bar{4}4}^2}{c_{44}}$	0

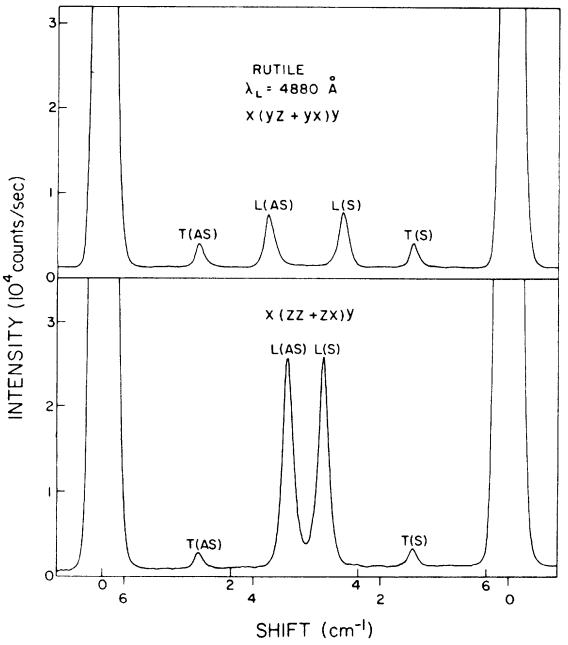

FIG. 2. Room-temperature Brillouin spectra of rutile observed with a triple passed scanning Fabry-Perot interferometer and excited with the multimode 4880-Å Ar^+ radiation incident along x (1,0,0) and scattered along y (0,1,0). The scales below and above the base line refer to the shifts of the Stokes (S) and the anti-Stokes (AS) components, respectively. T (transverse) and L (longitudinal) give the polarization characteristics of the phonon responsible for the scattering. The upper and lower portions of the figure were recorded with the incident polarization parallel and perpendicular to the scattering plane, respectively.

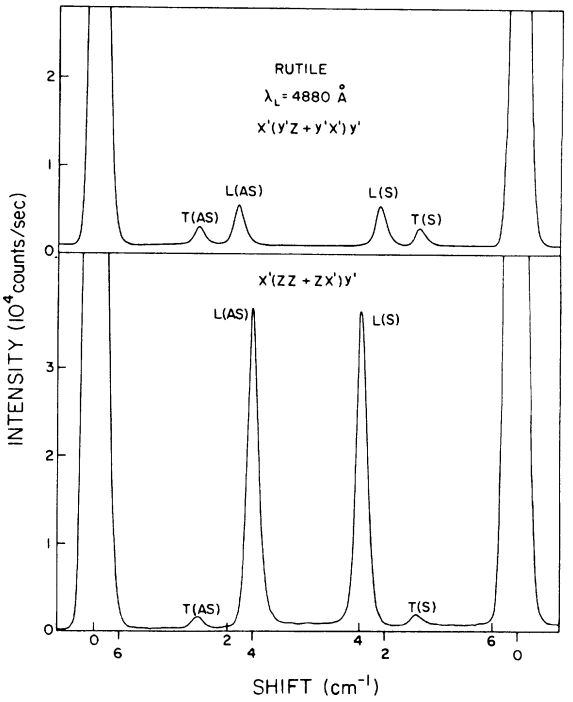

FIG. 3. Conditions under which these spectra were recorded are identical to those of Fig. 2 except that the incident radiation was along x' $[(-1/\sqrt{2}),(1/\sqrt{2}),0]$ and scattered along y' $[(1/\sqrt{2}),(1/\sqrt{2}),0]$.

volume demagnification, and the transmission factors at the entrance and exit faces. Both (ii) and (iii) have been discussed by Nelson, Lazay, and Lax.[6] In the interpretation of our results all these factors have been incorporated.

In Table IV we give the intensities of the Brillouin components for two of the scattering geometries extensively studied.

IV. EXPERIMENTAL RESULTS AND DISCUSSION

A. Elastic moduli

Figures 2 and 3 show the Brillouin spectra for two of the scattering geometries we have extensively studied. In Fig. 2, the incident and scattered directions are along x (1, 0, 0) and y (0, 1, 0), respectively; thus the phonon propagation direction is along $(1/\sqrt{2})(1, \bar{1}, 0)$ provided the incident and scattered light are both vertically or horizontally polarized. Here vertical (V) and horizontal (H) are defined with respect to the horizontal scattering plane. In Fig. 3, the results are for incident light along $(1/\sqrt{2})(\bar{1}, 1, 0)$ and scattered along $(1/\sqrt{2})(1, 1, 0)$, selecting a phonon propagation direction along (1, 0, 0) for both the incident and scattered polarizations either vertical or horizontal and designated VV and HH. Both figures dramatically illustrate the role of birefringence in the frequency shifts of Brillouin components. From Table IV it is at once evident that the longitudinal components occur in the VV or the HH polarizations; the lines which have these polarizations have been accordingly labeled as L and exhibit a larger frequency shift when the polarization of the incident light is changed from H to V. The designation S and AS refer to Stokes and anti-Stokes, respectively. It is clear that for these geometries HH and VV correspond to $n_i = n_s = n_o$ and $n_i = n_s = n_e$, respectively, hence the frequency shifts deduced from Eq. (2) will be in the ratio of $n_o : n_e$. For $\lambda_L = 4880$-Å exciting radiation, this ratio is 0.893 in excellent agreement with the shifts of the lines labeled L in Figs. 2 and 3. From Table IV it can be seen that the transverse T Brillouin components occur in the VH and HV polarizations and hence are produced by phonons propagating in directions making an angle of $\pm 3.2^\circ$ with the bisector in the xy plane. The symmetry of the geometries under consideration results in

TABLE V. Refractive indices of rutile (Ref. 4), fused quartz (Ref. 29), and glycerine (Ref. 28) at various wavelengths. n_o and n_e are the ordinary and extraordinary refractive indices and n_e' is the extraordinary refractive index for light propagating at 45° to the optic axis of rutile.

λ (Å)	6328	5145	4880	4579
Rutile (n_o)	2.584	2.690	2.731	2.793
Rutile (n_e)	2.872	3.006	3.059	3.138
Rutile (n_e')	2.717	2.835	2.881	2.950
Fused quartz (n_{FQ})	1.4570	1.4616	1.4630	1.4650
Glycerine (n_G)	1.4714	1.4766	1.4783	1.4805

the phonons on either side of the bisector being equivalent. For this reason, noting that Eq. (2) is symmetric in n_i and n_s, the splittings observed for HV and VH are identical as experimentally observed in Figs. 2 and 3.

The procedures followed in the determination of elastic moduli are described in our earlier paper on diamond.[3] In addition, for experiments with light incident along (0, 0, 1), conoscopic figures[19] allowed a higher degree of precision in the alignment of the sample. This proved to be especially important for the study of phonons which did not have an extremum in the angular dependence of their velocity in the vicinity of the direction under study. In our studies, we used both right-angle and back-scattering geometries. In the calculation of the X's we have used $\rho = 4.2493 \pm 0.0005$ g/cm^3, as determined by Straumanis, Ejima, and James.[20] The refractive indices were calculated from the dispersion formulae given by DeVore[4] and are presented in Table V.

Our experimental results for various combinations of c_{ij}'s are given in Table VI. A least-squares fit[21, 22] was made to the first seven entries in order to obtain c_{11}, c_{33}, c_{44}, c_{66}, and c_{12};

TABLE VI. Elastic moduli of rutile from Brillouin scattering (units: 10^{12} dyn/cm^2). R, L, M, and N are defined in Table III.

X	Experiment	Least-squares fit
c_{11}	2.674 ± 0.002	2.674 ± 0.002
c_{33}	4.790 ± 0.002	4.790 ± 0.002
c_{44}	1.232 ± 0.008	1.233 ± 0.008
c_{66}	1.886 ± 0.020	1.894 ± 0.015
$\frac{1}{2}(c_{11}+2c_{66}+c_{12})$	4.134 ± 0.016	4.135 ± 0.035
$\frac{1}{2}(c_{66}+c_{44})$	1.571 ± 0.013	1.564 ± 0.012
$\frac{1}{4}(c_{11}-c_{12}+2c_{44})$	0.832 ± 0.013	0.833 ± 0.014
$\frac{1}{2}(R+\sqrt{L})$	3.91 ± 0.15	3.993 ± 0.023
$\frac{1}{2}(R-\sqrt{L})$	1.036 ± 0.008	1.033 ± 0.023
$\frac{1}{2}(M-\sqrt{N})$	1.482 ± 0.008	1.489 ± 0.033

c_{13} was calculated using the values thus obtained and the remaining three combinations of c_{ij}'s. The column labeled "Least-squares fit" lists the calculated values of X's using the results of the least-squares fit; the agreement with the experimental values shows the excellent internal consistency of our results. Table VII shows the complete set of elastic moduli obtained in this investigation. Also listed are the previous determinations of these constants by other techniques.[23-25] It is gratifying to note that our values agree with the most accurate previous determination by Wachtman, Tefft, and Lam.[23]

We have calculated the Debye temperature Θ_D using our values of c_{ij}'s and a procedure of averaging the appropriate sound velocities for 400 propagation directions in one octant.[26] We obtain $\Theta_D = 758 \pm 6$°K which is to be compared with $\Theta_D = 778 \pm 5$ °K deduced by Sandin and Keesom[27] from specific-heat measurements. Robie and Edwards[26] have calculated $\Theta_D = 775$ °K using c_{ij}'s of Ref. 24;

TABLE VII. Elastic moduli of rutile (units: 10^{12} dyn/cm^2).

Method	c_{11}	c_{33}	c_{44}	c_{66}	c_{12}	c_{13}	Ref.
Brillouin scattering (~23 °C)	2.674 ±0.002	4.790 ±0.002	1.233 ±0.008	1.894 ±0.015	1.808 ±0.037	1.466 ±0.029	Present study
Ultrasonic resonance	2.660 ±0.066	4.699 ±0.081	1.239 ±0.007	1.886 ±0.050	1.733 ±0.071	1.362 ±0.081	23
Ultrasonic pulse technique	2.73	4.84	1.25	1.94	1.76	1.49	24
Ultrasonic pulse technique	2.48 ±0.08	4.52 ±0.08	1.20 ±0.03	1.6 ±0.1	2.0 ±0.1	1.4 ±0.1	25

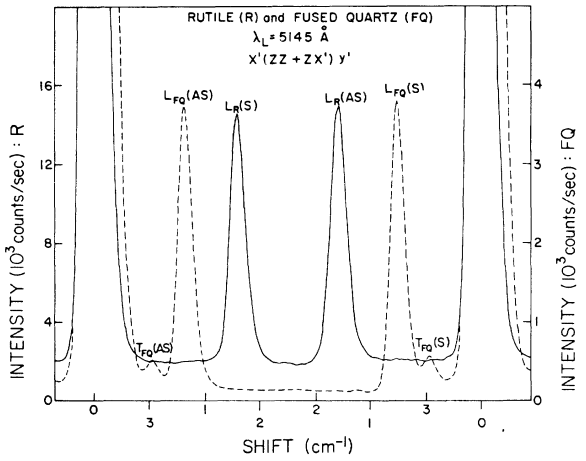

FIG. 4. Brillouin spectra of rutile (R), solid line, and fused quartz (FQ), dashed line, taken under identical experimental conditions. The spectra were recorded using 5145-Å incident radiation. The scattering geometry for the rutile sample is the same as that used to obtain Fig. 3.

the increase from 758 to 775 °K arises from the differences in the values for c_{ij}'s used. We feel that the accuracy of the results in the present investigation suggests that the difference between Θ_D obtained from our room-temperature c_{ij}'s and that obtained from low-temperature specific-heat data, is due to changes in c_{ij}'s as the temperature is decreased.

B. Elasto-optic constants: Comparison with fused quartz

The absolute values of several of the elasto-optic constants of rutile were deduced from an intercomparison of the intensities of the Brillouin components of rutile and fused quartz. For fused quartz, the intensity (I) of the longitudinal Brillouin component with incident light vertically polarized is proportional to $4n^8p_{12}^2/c_{11}$; the intensities of the Brillouin components of rutile for some of the geometries studied are given in Table IV. The constants of proportionality associated with the intensity expressions for the Brillouin components are the same for fused quartz and rutile.

The Brillouin spectra of fused quartz and rutile were recorded in the right-angle scattering geometry. Figure 4 shows typical spectra from which the experimental results were obtained. These were recorded with 5145-Å exciting radiation, the scattering geometry for rutile being the same as that used in Fig. 3. Since the intensity of the exciting radiation inside the sample is affected by the contributions from the reflections at the surfaces, the effect was minimized by immersing the samples in glycerine. Table V lists the refractive indices of glycerine[28] and fused quartz[29] used in the reduction of our data. We have used $p_{12} = +0.270$ for fused quartz which has a very small wavelength dependence as determined by Primak and Post.[30] Also, $c_{11} = 7.8394 \times 10^{11}$ dyn/cm^2 obtained by Bogardus[31] for fused quartz was used in our calculations. In Table VIII we give the results obtained after incorporating appropriate corrections for solid angle and transmission. In Table IX we summarize the elasto-optic constants found in the literature.[16, 17, 32-34] As can be seen, the agreement between our values in Table VIII and those in Table IX is reasonable. Using our values of $|p_{12}|$ and $|p_{13}|$, we find that agreement with the combination labeled A in Table VIII can be achieved only if p_{12} and p_{13} have opposite signs. With this assumption, the calculated

TABLE VIII. Elasto-optic constants of rutile obtained from an intercomparison with the Brillouin scattering in fused quartz. The values of $|p_{31}|$ were obtained with $\vec{k}_i \| (1/\sqrt{2})(\bar{1}, 1, 0)$, $\vec{k}_s \| (1/\sqrt{2})(1, 1, 0)$ and $\vec{k}_i \| (1, 0, 0)$, $\vec{k}_s \| (0, 1, 0)$; $|p_{12}|$ with $\vec{k}_i \| (1/\sqrt{2})(\bar{1}, 0, 1)$, $\vec{k}_s \| (1/\sqrt{2})(1, 0, 1)$; $|p_{13}|$ with $\vec{k}_i \| (1/\sqrt{2})(1, 0, \bar{1})$, $\vec{k}_s \| (1/\sqrt{2})(1, 0, 1)$; A with $\vec{k}_i \| (0, 0, 1)$, $\vec{k}_s \| (1, 0, 0)$, and B with $\vec{k}_i \| (0, 0, 1)$, $\vec{k}_s \| (1/\sqrt{2})(\bar{1}, \bar{1}, 0)$. A and B refer to intensities of quasitransverse phonons whereas the rest of the p_{ij}'s are related to the intensity scattered by longitudinal phonons. All the lines studied were in the VV polarization. $A = |\frac{1}{2}(1.1671p_{12} - 0.7986p_{13})|$; $B = |\frac{1}{2}[0.5285(p_{11} + p_{12}) - 0.9405p_{13} - 1.0570p_{66}]|$.

λ (Å)	6328	5145	4880	4579
$\lvert p_{31}\rvert$	0.090 ± 0.008	0.106 ± 0.008	0.112 ± 0.008	0.128 ± 0.009
$\lvert p_{12}\rvert$	0.144 ± 0.010	0.110 ± 0.014	0.102 ± 0.014	0.082 ± 0.014
$\lvert p_{13}\rvert$	0.140 ± 0.009	0.18 ± 0.02	0.19 ± 0.02	0.20 ± 0.02
A	0.14 ± 0.02	0.13 ± 0.02	0.13 ± 0.02	0.13 ± 0.02
B	0.15 ± 0.02	0.15 ± 0.02	0.15 ± 0.02	0.15 ± 0.02

TABLE IX. Elasto-optic constants of rutile from previous determinations.

λ (Å)	p_{11}	p_{12}	p_{13}	p_{33}	p_{31}	p_{44}	$p_{4\bar{4}}$	p_{66}	Ref.
6328	−0.011	+0.172	−0.168	−0.058	−0.0965				32 [a]
6328	−0.008	+0.17	−0.16	−0.062	−0.095			±0.071	33 [a]
5145					±0.0959	−0.0009	+0.0255	±0.0716	16, 17

[a] The signs of the p_{ij}'s follow Ref. 34. Note, however, that the sign of p_{11} has not been determined unambiguously.

values for A are 0.140 ± 0.010, 0.135 ± 0.017, 0.134 ± 0.017, and 0.126 ± 0.017 at 6328, 5145, 4880, and 4579 Å, respectively. The agreement with the measured values in Table VIII is seen to be excellent. The opposite signs of p_{12} and p_{13} as determined by our results agree with the results of Ref. 34, and hence we assign the same signs as determined in that paper to our values of p_{12} and p_{13}. In this respect we would like to point out that in Ref. 16 it was found that $|0.828p_{12} + 0.564p_{13}| = 0.237$. This is in striking contradiction to the assumption that p_{12} and p_{13} have opposite signs. It appears that this discrepancy is due to an error in the sign of the second term in their expression for the intensity.

C. Elasto-optic constants: Ratios of intensities of Brillouin components

From Table IV it is clear that ratios of elasto-optic constants can be deduced from the relative intensities of the Brillouin components. We have summarized in Table X these ratios obtained from various scattering geometries for different exciting wavelengths. Many of the ratios show a strong wavelength dependence. For example Fig. 5 shows the strong wavelength dependence found in one of the measured intensity ratios, where the incident and scattered radiation are along z (0,0,1) and x (1,0,0), respectively, and the incident polarization was along y (0,1,0). The upper- and lower-halves of the figure were recorded with 6328- and 4579-Å exciting radiation. The ratio of intensities of the quasitransverse to the quasilongitudinal is found to change from >120 to 10.2 ± 1.0 when the spectra are excited with 6328- and 4579-Å radiation, respectively. The elasto-optic constants determined from the ratios in Table X together with the p_{ij}'s of Table VIII are given in Table XI.

The following considerations were used in the preparation of Table XI. The elasto-optic constants p_{12} and p_{13} were determined from a least-squares fit of p_{12}, p_{13}, and A from Table VIII and ratios 13 and 15 in Table X; as mentioned earlier, the signs of p_{12} and p_{13} are opposite and taken to be positive and negative, respectively, to conform to Ref. 34. Note that two sets of values are given for ratio 8 in Table X; the lower set was selected to determine p_{33} since the values obtained with this choice agree with those given in Refs. 32 and 33. It can be seen that p_{33} and p_{13} have the same sign as indicated by the sign of the ratio. On the basis of ratios 2, 6, and 7 we conclude that $|p_{11}|$ is much smaller than $|p_{12}|$ and $|p_{13}|$. The above ratios also allow a rough determination of p_{11} which is given in Table XI. It is not possible to determine the sign of p_{31} from our data; the negative sign chosen for it in Table XI follows the results of Ref. 34.

As discussed in Secs. I and III, the symmetry of the elasto-optic constants as reformulated by Nelson and Lax[7] and by Anastassakis and Burstein[8] results in $p_{44} \neq p_{4\bar{4}} \neq p_{\bar{4}4} \neq p_{\bar{4}\bar{4}}$, and $p_{66} \neq p_{6\bar{6}}$. Within our experimental accuracy we find $p_{66} = p_{6\bar{6}}$ and hence an average obtained from ratios 5, 10, 16, and 18 in Table X is given in Table XI. The entry labeled B in Table VIII allows us to determine the sign of p_{66} to be negative. Figure 6 illustrates the intensity changes ascribable to $p_{\bar{4}\bar{4}} \neq p_{44}$. In the upper part of the figure the scattering geometry is that used in Fig. 2 and the incident light is horizontally polarized. From Table IV it is clear that the intensity of the transverse Brillouin component is proportional to $p_{\bar{4}\bar{4}}^2$. The lower-half corresponds to incident and scattered light along x' $[(1/\sqrt{2}), 0, (-1/\sqrt{2})]$ and z' $[(1/\sqrt{2}), 0, (1/\sqrt{2})]$, respectively, and horizontally polarized incident radiation. It can be shown that a transverse phonon should produce a Brillouin component at the positions labeled T with an intensity proportional to p_{44}^2. The absence of this line in the observed spectrum clearly indicates that p_{44} is considerably smaller than $p_{\bar{4}\bar{4}}$ in agreement with the results of Ref. 16. The lines labeled a, a', b, b' in the lower part of the figure arise from the incident radiation reflected at the exit face of the crystal and which in turn suffers Brillouin scattering; since different phonons are selected by the reflected radiation, the frequency shifts are correspondingly changed. From ratios 4 and 12 in Table X it is clear that $p_{\bar{4}\bar{4}} \neq p_{4\bar{4}}$. This

TABLE X. Ratios of elasto-optic constants obtained from Brillouin scattering studies. In this table L, T, QL, and QT refer to the polarization of the phonon, longitudinal, transverse, quasilongitudinal, and quasitransverse, respectively. The subscripts V and H refer to the polarization of the incident light relative to the horizontal scattering plane. Hence for example, T_H: QL_H indicates that the ratio of p_{ij}'s is obtained from the relative intensities of the transverse and quasilongitudinal components with the incident light horizontally polarized.

No.	k_i	k_s	Phonons	Ratio	6328 Å	5145 Å	4880 Å	4579 Å
1	$\frac{1}{\sqrt{2}}(\bar{1},1,0)$	$\frac{1}{\sqrt{2}}(1,1,0)$	$\frac{L_V}{T_{2V}}$	$\frac{\lvert p_{31}\rvert}{\lvert p_{44}\rvert}$	•••	4.52 ± 0.14	4.32 ± 0.13	4.45 ± 0.32
2	$\frac{1}{\sqrt{2}}(\bar{1},1,0)$	$\frac{1}{\sqrt{2}}(1,1,0)$	$\frac{L_V}{L_H}$	$\frac{\lvert p_{31}\rvert}{\lvert p_{11}-p_{12}\rvert}$	0.619 ± 0.019	0.878 ± 0.046	1.02 ± 0.08	1.27 ± 0.25
3	$\frac{1}{\sqrt{2}}(\bar{1},1,0)$	$\frac{1}{\sqrt{2}}(1,1,0)$	$\frac{L_H}{T_{2H}}$	$\frac{\lvert p_{11}-p_{12}\rvert}{\lvert p_{44}\rvert}$	>7.5	4.54 ± 0.07	3.88 ± 0.08	3.15 ± 0.05
4	$\frac{1}{\sqrt{2}}(\bar{1},1,0)$	$\frac{1}{\sqrt{2}}(1,1,0)$	$\frac{T_{2H}}{T_{2V}}$	$\frac{\lvert p_{44}\rvert}{\lvert p_{44}\rvert}$	•••	1.12 ± 0.08	1.17 ± 0.05	1.14 ± 0.07
5	$\frac{1}{\sqrt{2}}(\bar{1},0,1)$	$\frac{1}{\sqrt{2}}(1,0,1)$	$\frac{L_V}{T_{1V}}$	$\frac{\lvert p_{12}\rvert}{\lvert p_{66}\rvert}$	2.25 ± 0.17	1.74 ± 0.02	1.46 ± 0.14	1.08 ± 0.06
6	$\frac{1}{\sqrt{2}}(\bar{1},0,1)$	$\frac{1}{\sqrt{2}}(1,0,1)$	$\frac{L_V}{L_H}$	$\frac{\lvert p_{12}\rvert}{a_1}$	2.28 ± 0.07	•••	•••	•••
7	$\frac{1}{\sqrt{2}}(\bar{1},0,1)$	$\frac{1}{\sqrt{2}}(1,0,1)$	$\frac{L_H}{T_{1H}}$	$\frac{a_2}{\lvert p_{66}\rvert}$	1.29 ± 0.05	1.24 ± 0.03	1.25 ± 0.05	1.24 ± 0.14
8	$\frac{1}{\sqrt{2}}(1,0,\bar{1})$	$\frac{1}{\sqrt{2}}(1,0,1)$	$\frac{L_V}{L_H}$	$\frac{p_{33}}{p_{13}}$	1.639 ± 0.034 0.408 ± 0.034	1.621 ± 0.028 0.383 ± 0.028	1.601 ± 0.029 0.384 ± 0.029	1.557 ± 0.024 0.403 ± 0.024
9	(1, 0, 0)	(0, $\bar{1}$, 0)	$\frac{L_V}{T_{2V}}$	$\frac{\lvert p_{31}\rvert}{\lvert p_{44}\rvert}$	•••	4.36 ± 0.08	4.29 ± 0.07	4.26 ± 0.04
10	(1, 0, 0)	(0, $\bar{1}$, 0)	$\frac{L_V}{L_H}$	$\frac{\lvert p_{31}\rvert}{\frac{1}{2}(\lvert p_{66}+p_{66}\rvert)}$	1.38 ± 0.03	1.59 ± 0.02	1.62 ± 0.04	1.74 ± 0.08
11	(1, 0, 0)	(0, $\bar{1}$, 0)	$\frac{L_H}{T_{2H}}$	$\frac{\frac{1}{2}(\lvert p_{66}+p_{66}\rvert)}{\lvert p_{44}\rvert}$	2.71 ± 0.08	2.40 ± 0.05	2.23 ± 0.07	2.11 ± 0.02
12	(1, 0, 0)	(0, $\bar{1}$, 0)	$\frac{T_{2H}}{T_{2V}}$	$\frac{\lvert p_{44}\rvert}{\lvert p_{44}\rvert}$	•••	1.18 ± 0.02	1.22 ± 0.04	1.15 ± 0.04
13	(0, 0, 1)	($\bar{1}$, 0, 0)	$\frac{QT_V}{QL_V}$	$\frac{a_3}{a_4}$	>5.6	2.56 ± 0.18	2.05 ± 0.06	1.62 ± 0.08
14	(0, 0, 1)	($\bar{1}$, 0, 0)	$\frac{T_H}{QL_H}$	$\frac{\lvert p_{66}\rvert}{a_5}$	>2.3	3.20 ± 0.27	3.06 ± 0.22	2.34 ± 0.29
15	($\bar{1}$, 0, 0)	(0, 0, 1)	$\frac{QT_V}{QL_V}$	$\frac{a_3}{a_4}$	>4.5	2.52 ± 0.04	1.96 ± 0.03	1.46 ± 0.04
16	($\bar{1}$, 0, 0)	(0, 0, 1)	$\frac{T_V}{QL_V}$	$\frac{\sqrt{2}\lvert p_{66}\rvert}{a_4}$	•••	0.89 ± 0.04	0.71 ± 0.02	0.61 ± 0.02
17	($\bar{1}$, 0, 0)	(0, 0, 1)	$\frac{QT_H}{QL_H}$	$\frac{a_6}{a_7}$	•••	1.08 ± 0.10	0.82 ± 0.05	0.56 ± 0.01
18	($\bar{1}$, 0, 0)	(0, 0, 1)	$\frac{T_V}{QT_V}$	$\frac{\sqrt{2}\lvert p_{66}\rvert}{a_3}$	0.29 ± 0.01	0.35 ± 0.01	•••	•••

TABLE X. (*continued*)

$a_1 = |-0.610p_{11} + 0.597p_{31}|$ at 6328 Å

$a_2 = |-0.781p_{11} + Ap_{31}|$ $\left[A = 0.763,\ 0.780,\ 0.787,\ \text{and } 0.797 \text{ at } 6328,\ 5145,\ 4880,\ \text{and } 4579 \text{ Å, respectively.}\right]$

$a_3 = |1.1672p_{12} - 0.7986p_{13}|$

$a_4 = |0.7986p_{12} + 1.1672p_{13}|$

$a_5 = |0.8423p_{\bar{4}\bar{4}} + 0.5670p_{\bar{4}\bar{4}}|$

$a_6 = |-0.4484p_{4\bar{4}} + 0.5325p_{44}|$

$a_7 = |0.5956p_{4\bar{4}} + 0.4009p_{44}|$

is the first verification of the prediction of Ref. 8, that $p_{ijkl} \neq p_{jikl}$. Using the values of $|p_{31}|$, $|p_{11} - p_{12}|$, and $\frac{1}{2}|p_{66} + p_{6\bar{6}}|$ determined in this investigation, a least-squares fit is made to ratios 1, 3, 4, 9, 11, and 12 to obtain $|p_{\bar{4}\bar{4}}|$ and $|p_{4\bar{4}}|$. These are given in Table XI. From ratio 17, $|p_{44}|$ was calculated to be 0.0048 ± 0.0015, 0.0012 ± 0.0010, and 0.0045 ± 0.0005 for 5145-, 4880-, and 4579-Å exciting radiation; also p_{44} has a sign opposite to that of $p_{4\bar{4}}$ at 5145 and 4880 Å and the same sign at 4579 Å. Ratio 14 permits us to establish that $p_{\bar{4}4} \ll p_{\bar{4}\bar{4}}$. Nelson and Lazay[16,17] have obtained $p_{44} = -0.0009$, $p_{\bar{4}\bar{4}} = 0.0257$, and $p_{4\bar{4}} = 0.0253$ at 5145 Å. It is important to draw attention to the fact that they did not observe a significant difference between $p_{\bar{4}\bar{4}}$ and $p_{4\bar{4}}$. It is possible to calculate $(p_{44} - p_{4\bar{4}})$ and $(p_{\bar{4}4} - p_{\bar{4}\bar{4}})$ in terms of the refractive indices as shown by Nelson and Lax.[7] Using their Eq. (8) in which no explicit assumption has been made regarding the symmetry of the first two indices of p_{ijkl} we obtain

$$p_{13[13]} = \tfrac{1}{2}(p_{44} - p_{4\bar{4}}) = \tfrac{1}{2}(1/n_e^2 - 1/n_0^2) \qquad (5)$$

and

$$p_{31[13]} = \tfrac{1}{2}(p_{\bar{4}4} - p_{\bar{4}\bar{4}}) = \tfrac{1}{2}(1/n_e^2 - 1/n_0^2). \qquad (6)$$

Here the [ ] denotes the antisymmetry of the indices involved. Table XII compares the predictions of Eq. (5), with our experimental results. In order to obtain the excellent agreement seen in Table XII, it is necessary to assume, following Nelson and Lazay,[16,17] that $p_{4\bar{4}}$ is positive. With the sign of $p_{4\bar{4}}$ thus fixed, the analysis of ratio 17 in Table X yields the sign of p_{44} given in Table XI. It is interesting to note the change in the sign of p_{44} in going from 5145 to 4579 Å. The values for $p_{\bar{4}4}$ given in Table XI are obtained from $\frac{1}{2}(1/n_e^2 - 1/n_0^2)$ and $p_{\bar{4}\bar{4}}$ using Eq. (6).

D. Relative intensities of Raman and Brillouin spectra

Figure 7 shows the Brillouin spectrum and the 447-cm^{-1} first-order Raman line of E_g symmetry of rutile[35] recorded under identical experimental

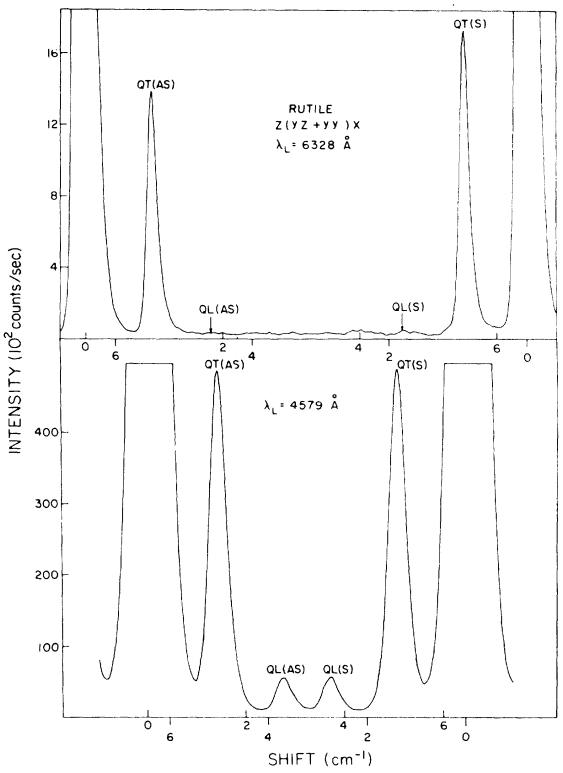

FIG. 5. Brillouin scattering in rutile as a function of wavelength of the exciting radiation. $\vec{k}_i \parallel (0,0,1)$ and $\vec{k}_s \parallel (1,0,0)$ with the incident polarization vertical, i.e., along (0, 1, 0). The upper- and lower-halves of the figure were recorded with ~ 80 mW of 6328-Å and ~ 250 mW of 4579-Å exciting radiation, respectively.

TABLE XI. Elasto-optic constants of rutile obtained from a Brillouin scattering investigation.

λ (Å)	6328	5145	4880	4579
p_{12}	+0.144 ± 0.010	+0.113 ± 0.009	+0.100 ± 0.008	+0.078 ± 0.006
p_{13}	−0.140 ± 0.009	−0.167 ± 0.013	−0.183 ± 0.014	−0.194 ± 0.015
p_{33}	−0.057 ± 0.009	−0.064 ± 0.010	−0.070 ± 0.011	−0.078 ± 0.011
$p_{66} \cong p_{6\bar{6}}$	−0.062 ± 0.005	−0.066 ± 0.004	−0.068 ± 0.006	−0.073 ± 0.006
p_{31}	−0.090 ± 0.008	−0.106 ± 0.008	−0.112 ± 0.008	−0.128 ± 0.009
$p_{4\bar{4}}$	•••	+0.0237 ± 0.0013	+0.0255 ± 0.0014	+0.0300 ± 0.0015
$p_{4\bar{4}}$	+0.023 ± 0.003	+0.0277 ± 0.0015	+0.0304 ± 0.0017	+0.0344 ± 0.0018
p_{44}	•••	−0.0048 ± 0.0015	−0.0012 ± 0.0010	+0.0045 ± 0.0005
$p_{\bar{4}4}$	−0.006 ± 0.003	+0.0001 ± 0.0015	+0.0032 ± 0.0017	+0.0078 ± 0.0018
p_{11}	+0.012 ± 0.015	−0.001 ± 0.018	−0.005 ± 0.021	−0.017 ± 0.034

conditions with a grating double monochromator[36]; the results are corrected for the instrument function. The scattering geometry used is the same as that in Fig. 2 with incident light vertically polarized. From Table IV, it can be seen that the longitudinal Brillouin component appears only in the VV polarization. The scattering efficiency of the longitudinal Brillouin component S per unit crystal length, per unit solid angle at temperature T can be shown to be[37]

$$S(\text{Brillouin}_L) = \frac{kT\omega_s^4}{128\pi^2 c^4} \frac{8n_e^8 p_{31}^2}{c_{11}+c_{12}+2c_{66}}, \quad (7)$$

where ω_s is the frequency of the scattered light. The scattering efficiency for the Raman lines may be defined by the following equation:

$$S(\text{Raman}) = K(\hat{e}_s \cdot \underline{T} \cdot \hat{e}_i)^2, \quad (8)$$

where $\underline{T}$ is the appropriate Raman tensor.[37] From a comparison of Eq. (8) above and Eq. (4) of Ref. 3 for the zone-center optical phonon of diamond we obtain

$$K = (2\hbar\omega_s^4 N^2/\rho c^4 \omega_j)(n_0+1), \quad (9)$$

where N is the number of primitive cells per unit volume, n_0 is the Bose population factor, and ω_j is the frequency of the Raman line. It should be noted that K has been deduced for the zone-center optical phonon for diamond by Smith from a microscopic description of the normal mode.[38] Since we have not carried out a corresponding calculation for the 447-cm^{-1} E_g line of rutile, the single constant d characterizing the Raman tensor per unit cell should only be regarded as an experimentally determined parameter. For the geometry used in Fig. 7, it can be shown using the Raman tensors given in Ref. 35,

$$S(\text{Raman}) = (2\hbar\omega_s^4 N^2 d^2/\rho c^4 \omega_j)(n_0+1). \quad (10)$$

From our experimental results we find that the ratio of the integrated intensity of the Raman line

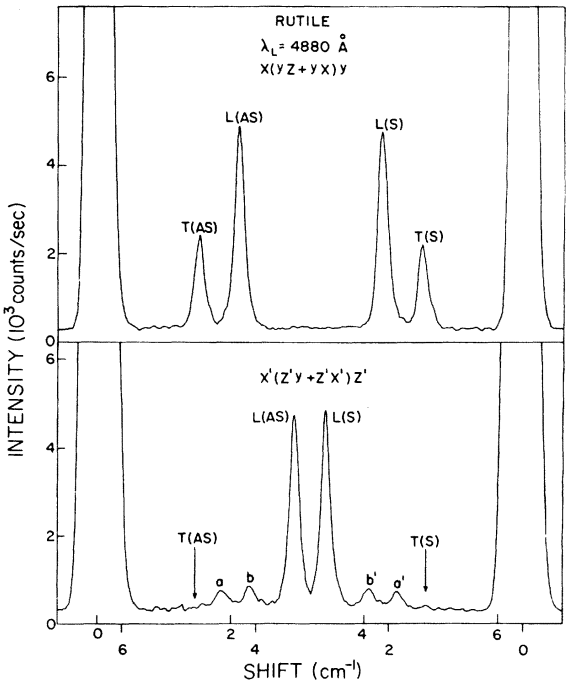

FIG. 6. Brillouin scattering spectra of rutile, illustrating the dramatic changes in intensities due to the recently predicted (Refs. 7 and 16) changes in the p_{ij}'s. In the upper-half of the figure the scattering geometry is that of Fig. 2 and the incident light is horizontally polarized. The lower-half corresponds to incident and scattered light along x' $[(1/\sqrt{2}), 0, (-1/\sqrt{2})]$ and z' $[(1/\sqrt{2}), 0, (1/\sqrt{2})]$, respectively, and horizontally polarized incident radiation. The arrows indicate the positions at which the transverse components for this geometry are expected. The lines labeled a, a', b, and b' can be traced to the presence of a reflected laser beam from the exit face of the sample. The spectra were recorded with 4880-Å exciting radiation.

TABLE XII. Rotational contribution to Brillouin scattering calculated from Eq. (5) using the refractive indices given in Table V. In order to obtain the agreement in sign, it is necessary to assume that the sign of p_{44} is positive.

λ (Å)	6328	5145	4880	4579
Calc.	−0.0143	−0.0138	−0.0136	−0.0133
Expt.	•••	−0.0143 ± 0.0014	−0.0134 ± 0.0012	−0.0128 ± 0.0010

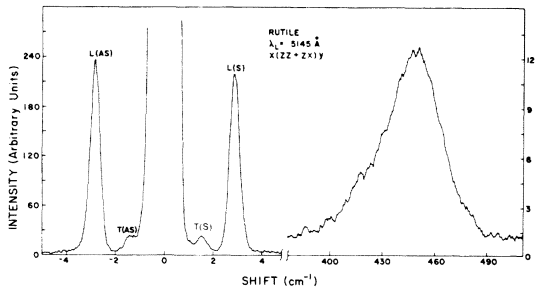

FIG. 7. Brillouin spectrum and the 477-cm^{-1} first-order Raman line of rutile recorded with the scattering geometry of Fig. 2. The spectra were obtained using vertically polarized 5145-Å exciting radiation under identical experimental conditions on a double monochromator. The data presented in this figure have been corrected for the instrument function.

to that of the longitudinal Brillouin component is 3.3 ± 0.6. In the determination of this ratio, we have taken into account the effects of solid angle and transmission factors described earlier. From Eqs. (7) and (10) we obtain $d = 22 \pm 2$ Å^2. using $N = 1.6 \times 10^{22}$ cm^{-3} calculated with the lattice parameters[39] and the other constants given in this paper.

ACKNOWLEDGMENTS

Our thanks are due to Dr. J. G. Bennett for the computer program used to calculate the Debye Θ. We wish to thank Professor S. Rodriguez for discussions and a critical reading of this manuscript.

*Work supported by the NSF under Grant No. GH 32001A1 and MRL Program Nos. DMR-7203018A03 and DMR7203018A04.

[1]H. Z. Cummins and P. E. Schoen, in *Laser Handbook*, edited by F. T. Arecchi and E. O. Schulz-Dubois (North-Holland, Amsterdam, 1972), p. 1029.

[2]D. Landheer, H. E. Jackson, R. A. McLaren, and B. P. Stoicheff, Phys. Rev. B 13, 888 (1976).

[3]M. H. Grimsditch and A. K. Ramdas, Phys. Rev. B 11, 3139 (1975).

[4]J. R. DeVore, J. Opt. Soc. Am. 41, 416 (1951).

[5]V. Chandrasekharan, Proc. Ind. Acad. Sci. A 33, 183 (1951).

[6]D. F. Nelson, P. D. Lazay, and M. Lax, Phys. Rev. B 6, 3109 (1972).

[7]D. F. Nelson and M. Lax, Phys. Rev. Lett. 24, 379 (1970).

[8]E. Anastassakis and E. Burstein, J. Phys. C 7, 1374 (1974).

[9]National Lead Co., Titanium Div., P. O. Box 58, South Amboy, N. J. 08879.

[10]Amersil Inc., 685 Ramsey Ave., Hillside, N. J. 07205.

[11]M. H. Grimsditch, Ph.D. thesis (Purdue University, 1976) (unpublished).

[12]See, for example, J. F. Nye, *Physical Properties of Crystals* (Oxford U. P., London, 1967).

[13]J. Laval, C. R. Acad. Sci. (Paris) 232, 1947 (1951); 238, 1773 (1954).

[14]K. S. Viswanathan, Proc. Ind. Acad. Sci. A 39, 196 (1954).

[15]C. V. Raman and K. S. Viswanathan, Proc. Ind. Acad. Sci. A 42, 1 (1955); 42, 51 (1955).

[16]D. F. Nelson and P. D. Lazay, Phys. Rev. Lett. 25, 1187 (1970).

[17]D. F. Nelson and P. D. Lazay, Phys. Rev. Lett. 25, 1638 (1970).

[18]M. Lax, *Symmetry Principles in Solid State and Molecular Physics* (Wiley, New York, 1974), p. 126.

[19]F. A. Jenkins and H. E. White, *Fundamentals of Optics* (McGraw-Hill, New York, 1957).

[20]M. E. Straumanis, T. Ejima, and W. J. James, Acta. Crystallogr. 14, 493 (1961).

[21]J. W. M. DuMond and E. R. Cohen, Rev. Mod. Phys. 25, 691 (1953).

[22]E. R. Cohen, Rev. Mod. Phys. 25, 709 (1953).

[23]J. B. Wachtman, W. E. Tefft, and D. G. Lam, J. Res. Natl. Bur. Std. (U.S.) 66A, 465 (1962).

[24]F. Birch, J. Geophys. Res. 65, 3855 (1960); see also R. K. Verma, *ibid.* 65, 757 (1960).

[25]G. L. Vick and L. E. Hollander, J. Acoust. Soc. Am. 32, 947 (1960).

[26]We have used the computer program developed by Dr. J. G. Bennett of our department. See also R. A. Robie and J. L. Edwards, J. Appl. Phys. 37, 2659 (1966).

[27]T. R. Sandin and P. H. Keesom, Phys. Rev. 177, 1370 (1969).

[28]*Smithsonian Physical Tables*, edited by W. E. Forsythe (The Smithsonian Institution, Washington, D.C., 1954), Table 551.

[29]I. H. Malitson, J. Opt. Soc. Am. 55, 1205 (1965).

[30]W. Primak and D. Post, J. Appl. Phys. 30, 779 (1959).

[31]E. H. Bogardus, J. Appl. Phys. 36, 2504 (1965).
[32]R. W. Dixon, J. Appl. Phys. 38, 5149 (1967).
[33]J. Reintjes and M. B. Schulz, J. Appl. Phys. 39, 5254 (1968).
[34]T. A. Davis and K. Vedam, J. Opt. Soc. Am. 58, 1446 (1968).
[35]S. P. S. Porto, P. A. Fleury, and T. C. Damen, Phys. Rev. 154, 522 (1967).
[36]Model 25-100 double monochromator, Jarrell-Ash Div., 590 Lincoln St., Waltham, Mass. 02154.
[37]R. Loudon, Adv. Phys. 13, 423 (1964).
[38]H. M. J. Smith, Philos. Trans. R. Soc. Lond. A 241, 105 (1948).
[39]*Structure Reports*, edited by W. B. Pearson (N. V. A. Oosthoek's Uitgevers Mij, Utrecht, 1968), Vol. 24, p. 311.